Journal of Magnetism and Magnetic Materials 543 (2022) 168608

Contents lists available at ScienceDirect

Journal of Magnetism and Magnetic Materials

journal homepage: www.elsevier.com/locate/jmmm

Research articles

# High-frequency magnetic response of superferromagnetic nanocomposites

Kacper Brzuszek, Andrzej Janutka *

*Department of Theoretical Physics, Wroclaw University of Science and Technology, 50-370 Wrocław, Poland*

ARTICLE INFO

*Keywords:*
Superferromagnetism
Power conversion
Micromagnetic simulations
Ferromagnetic resonance
High-frequency magnetic response

ABSTRACT

Studies of the dynamical response of thin-film composites of magnetic nanoparticles embedded in dielectric matrices to the oscillatory magnetic field of the microwave-frequency range are performed using numerical simulations. Four soft-magnetic systems; $(Co)_{0.42}(MgF_2)_{0.58}$, $(Fe_{65}Co_{35})_{0.57}(SiO_2)_{0.43}$, $(Fe_{65}Co_{35})_{0.75}(Al_2O_3)_{0.25}$, $(Fe_{65}Co_{35})_{0.6}(Al_2O_3)_{0.4}$, typical of a class of "high-frequency ferromagnetic nanocomposites" are simulated. The necessary micromagnetic parameters are extracted from data within the model of random magnetic anisotropy (RMA). Those materials are candidates for use in micro-converters of power (inductors and transformers) due to their high saturation magnetization, high resistivity, and absence of intra-grain magnetic domains. Thus, they are able to create a high magnetic flux at low power losses. The simulations allow for an inspection into details of the spatial distribution of the oscillating magnetization. We predict noticeable differences in the ferromagnetic resonance (FMR) in different composites which are related to the shape of the static hysteresis. Operating ranges of the driving-field amplitude are related to the hysteresis width. Next to FMR, we analyze the magnetic response via the oscillatory motion of domain walls in a longitudinal field. Besides the response to the alternating field of a constant direction, we study the magnetization dynamics driven by in-the-plane-rotating field. Such a field can drive the magnetization rotations which are a strong-response (nonlinear) mode potentially useful for efficient power conversion.

## 1. Introduction

Limitations of the semiconductor-based power electronics motivate the interest in the layers of soft-magnetic properties with a high resistivity for microinductors and transformers to be operated at high (near-microwave) frequencies [1–3]. This is because the miniaturization of the power converters is connected to a decrease of the magnetic flux which has to be compensated by an increase of the frequency [4,5]. The constant challenge in the field is the reduction of the power loss due to the fast remagnetizations. Present magnetic-core microconverters of power utilize the effect of the ferromagnetic resonance (FMR), while, being operated at considerably-lower frequencies than the FMR frequency, in a region far from the maximum of spin losses. Another way of the power conversion utilizes the oscillatory motion of domain walls (DWs) in a magnetic layer, however, its frequency is limited by the eddy-current (excess) losses and the skin effect [6]. Hence, the improvement of the high-frequency magnetic materials is related to the increase of the FMR frequency and/or the decrease of the electrical resistivity at the high permeability. Unfortunately, the Snoek and Acher laws are strong constraints impeding the former, while, the metallicity of the soft ferromagnets impedes the later [7–9].

For a long time, hopes for producing highly-permeable materials for the power conversion at low losses are connected with composites of high-magnetization nanoparticles embedded in dielectric matrices [1–3,10,11]. The major advantage of the magnetic-metal–dielectric nanocomposites is a very-high resistivity, (the residual-conductivity mechanism is related to the electron tunneling through the dielectric barriers between the metallic nanoparticles). Reducing the volume content of the metallic phase suppresses the inter-grain eddy currents, thus, reducing losses, (at a larger microwave permeability than that of ferrites [12]). Simultaneously, the magnetic grains (nanoparticles) are monodomain and small enough to suppress the circulation of the electric charge (due to eddy currents) or skin effect inside them, (unlike in ferrites [13] or other industrial soft-magnetic (micro)composites [11, 14]). On the other hand, the nonuniform spatial distribution of the magnetic moments can lead to deviations of FMR in the nanocomposites from typical of the films of homogeneous ferromagnets, which gives some hope for breaking the Snoek/Acher limit of the permeability value.

Nowadays, the class of manufactured ferromagnetic metal–dielectric nanocomposites is rich, and methods for enhancing the uniaxial anisotropy of their films (in order to increase the frequency of FMR)

* Corresponding author.
*E-mail address:* Andrzej.Janutka@pwr.edu.pl (A. Janutka).

https://doi.org/10.1016/j.jmmm.2021.168608
Received 14 January 2021; Received in revised form 22 September 2021; Accepted 25 September 2021
Available online 9 October 2021

are established; oblige deposition or deposition in a magnetic field [8]. In spite of this, at present, the operating regime of the nanogranular-core inductors is limited to MHz frequencies well below the microwave region, (they utilize FMR due to in-the-plane field), [15–17]. Independent of the eddy-current losses, the frequency is limited by spin losses and a decrease of the permeability. In the present paper, we explore the potential of several magnetic nanocomposites in terms of strengthening the magnetic response at the microwave frequencies via numerical simulations.

Manufacturing nanocomposite magnets is a complex process and it is not standardized. Possible clustering of the magnetic nanoparticles can result in creating paths for eddy-current conducting. Inhomogeneities of the magnetic ordering can result in the coexistence of different dynamical processes; FMR and DW motion, independent of the orientation of the driving field. Identifying the occurrence of these imperfections in the high-frequency dynamics requires the support from the knowledge of the dynamical response of the ideal systems, whereas, popular analytical models of FMR and oscillatory DW motion are oversimplified when applied to the nanocomposite [9]. Full experimental characterization of the radio-frequency properties is challenging since it requires performing different measurements in a wide range of frequencies. The simulations are helpful in completing data of particular experiments. We perform micromagnetic simulations of microwave dynamics of in-the-plane magnetized films of several magnetic-metal–dielectric nanocomposites of the "ultimate" purity. We mean the systems of uniformly dispersed magnetic nanoparticles in a uniform dielectric matrix without any electrical current, thus, with losses of the spin origin only. We study the magnetization oscillations driven by the magnetic longitudinal or transverse in-the-plane field as well as by in-the-plane-rotating field. We have three particular goals; checking the applicability of the analytical description of the transverse-field-driven FMR, determining the efficiency of DW-assisted response to the longitudinal driving field, and validating the strength and checking the periodicity of the response to rotating in-the-plane field.

High permeability of the nanogranular magnets requires the saturation magnetization of the system as a whole to be high, thus, the volume percentage of the magnetic phase has to be large at the expense of the distance of the granule separation. This results in an outflow of the spin density outside the metallic component into the dielectric matrix, making the spin system continuous and ferromagnetically ordered [18]. The basic role is believed to be played by (oxygen) vacancies in the matrix [19]. Note a similarity to an effect of appearance of the magnetization at the surface of nanoparticles of oxide (non-ferromagnetic) materials [20]. Detailed description of the magnetic ordering in metal–dielectric nanocomposites is performed within the models of the random magnetic anisotropy (RMA), which, developed for the amorphous magnets [21], is also a canonical approach to describing the nanogranular ferromagnets [22–24]. The analysis of the parameters of magnetic properties from data of static measurements allows us for formulating a "micromagnetic" model of the layered nanocomposites. Due to a smooth leakage of the spin from the ferromagnetic nanoparticles (small gradient of the magnetization), the demagnetizing field in the material body is negligible, however, the shape-anisotropy field of the easy-plane type (that confines the magnetization to the layer plane in the static case) is not.

In Section 2, we formulate the micromagnetic model of the metal–dielectric nanocomposite. Section 3 is devoted to characterizing the ordering in terms of the static hysteresis. The dynamical properties are studied in Section 4, and conclusions are summarized in Section 5.

## 2. Model

The dynamics of the ferromagnetic media is described with the Landau–Lifshitz–Gilbert (LLG) equation of the evolution of magnetization $\mathbf{M} = M_s\mathbf{m}$, ($M_s$ denotes the saturation magnetization)

$$-\frac{\partial \mathbf{m}}{\partial t} = \frac{2\gamma A_{ex}}{M_s}\mathbf{m}\times\Delta\mathbf{m} + \gamma\mathbf{m}\times(\mathbf{B}_{an}+\mathbf{B}) - \alpha\mathbf{m}\times\frac{\partial\mathbf{m}}{\partial t}, \tag{1}$$

the coefficients of whom are dependent on the spatial coordinates. Here, $\mathbf{B}_{an}$ and $\mathbf{B}$ denote the anisotropy field (relevant to local crystal structure) and an external field applied. The parameters; $\gamma$, $\alpha$ denote the gyromagnetic factor and the Gilbert damping constant, respectively. The random orientation of the crystallographic axes of the ferromagnetic nanoparticles results in a random distribution of the magnetic anisotropy directions within the layer. Inside the magnetic nanoparticles, values of the saturation magnetization $M_s = M_s^{(m)}$, the exchange stiffness $A_{ex} = A_{ex}^{(m)}$ and the anisotropy field $|\mathbf{B}_{an}| = |\mathbf{B}_{an}^{(m)}|$ are assumed to be almost the same as in the bulk of the ferromagnetic material. However, a leakage of a small amount of the spin from the nanoparticles into the dielectric matrix results in the formation of a continuous system of ferromagnetically-interacting magnetic moments. We evaluate values of $M_s = M_s^{(d)}$, $A_{ex} = A_{ex}^{(d)}$, $|\mathbf{B}_{an}| = |\mathbf{B}_{an}^{(d)}|$ relevant to the dielectric matrix, based on experimental data. Whereas, primary analysis of the experiments use mean values of the magnetization and of the exchange stiffness, we extract values relevant to the nanoparticles and to the matrix, applying the RMA model of structural ferromagnets [21–23].

For simplicity of the numerical discretization of the medium, we consider the ferromagnetic inclusions to be cubes of the edge length of $D$, ordered into a cubic lattice (of the lattice constant $D+\Lambda$) and we exclude the magnetostatic effects of the nanoparticle shape from the considerations. While, the RMA models are universal, the magnetostatics is very sensitive to the geometrical details. Beyond the nanoparticle shape and the diameter distribution, including the demagnetization requires detailed knowledge on the distribution of spin in the vicinity of the metal–dielectric interface whose changes are not jumpwise in real systems, (our test simulations including the demagnetization field with the sharp boundaries between the matrix and nanoparticles led to unphysical results).

All the necessary factors to determine the magnetic properties are believed to be contained in effective parameters of the RMA model: average saturation magnetization $\bar{M}_s$, effective exchange stiffness $\bar{A}_{ex}$, a constant of the local anisotropy $K_1$ (relevant to the nanoparticles), the constant of the global uniaxial anisotropy $K_u$, which are available from literature data. Knowing additionally the bulk values of the micromagnetic parameters for the inclusion material, we extract the values relevant to the dielectric matrix with dependence on the volume fraction of the ferromagnetic material $x$. For this purpose, first, we define the volume fraction of the dense ferromagnetic phase $x_p \equiv D^3/(D+\Lambda)^3$. Noticing the existence of a critical value of the volume fraction of the ferromagnetic material $x_c$, (the composite is spontaneously magnetized for $x \in (x_c, 1]$), we estimate $x_p \equiv (x-x_c)/(1-x_c)$, which satisfies $x_p \to_{x\to x_c^+} 0$ and $x_p \to_{x\to 1^-} 1$.

The effective exchange stiffness is evaluated with

$$\bar{A}_{ex} = \left(\frac{x_p\sqrt{K_u}K_1^2D^3}{\mu_0\bar{M}_sH_{cy}}\right)^{2/3}, \tag{2}$$

based on the formulas of the RMA model, where $H_{cy}$ denotes the coercive field of the "transverse hysteresis" which is obtained with the field directed onto the magnetically-hard axis ($y$ axis) [25]. From the relationships

$$\begin{aligned}\bar{M}_s &= x_pM_s^{(m)} + (1-x_p)M_s^{(d)},\\ \frac{D+\Lambda}{\sqrt{\bar{A}_{ex}}} &= \frac{D}{\sqrt{A_{ex}^{(m)}}} + \frac{\Lambda}{\sqrt{A_{ex}^{(d)}}}\end{aligned} \tag{3}$$

we extract

$$\begin{aligned}M_s^{(d)} &= \frac{\bar{M}_s - x_pM_s^{(m)}}{1-x_p}\\ A_{ex}^{(d)} &= \frac{\left(x_p^{-1/3}-1\right)^2\bar{A}_{ex}A_{ex}^{(m)}}{\left(x_p^{-1/3}\sqrt{A_{ex}^{(m)}} - \sqrt{\bar{A}}\right)^2}.\end{aligned} \tag{4}$$

At the nanoparticle–matrix interface, we apply the exchange-stiffness value of $A_{ex}^{(m)}$.

Finally, the anisotropy field can be written in the form

$$\mathbf{B}_{an} = \frac{2K_1}{M_s}(\mathbf{m}\cdot\hat{n})\hat{n} + \frac{2K_u}{M_s}(\mathbf{m}\cdot\hat{i})\hat{i} + \frac{2K}{M_s}(\mathbf{m}\cdot\hat{k})\hat{k}, \tag{5}$$

where $\hat{n}$ is a randomly-oriented unit vector that is constant inside each nanoparticle, $K_1$ is the anisotropy constant of the magnetic-component material, which is equal to zero in the matrix, $K_u$ is constant in whole the magnetic medium, and $K \equiv -\mu_0 \bar{M}_s^2/2$ denotes the constant of the effective easy-plane anisotropy.

In our numerical simulations, the choice of the magnetic nanoparticle material is motivated by the highest possible saturation magnetization and the simplicity of the chemical composition, as well as by the absence of the rare earth content. The highest available magnetization is offered by $Fe_{65}Co_{35}$, while, Co nanoparticles are also attractive in terms of the above criteria. Note that, while of a very high magnetization, Fe is not described with our model because of its cubic anisotropy. The requirement of a high strength of the uniaxial anisotropy of the nanocomposite is related to the technique of manufacturing rather than to the nanoparticle material and $K_u$ value in our simulations is dictated by the availability of experimental data. The same concerns the Gilbert damping constant which is extremely sensitive to the quality of the magnetic structure and its realistic value is far from one of the pure material. We use the relatively-high value $\alpha = 0.1$, which is quite typical of magnetic nanosystems with significant structural imperfections.

## 3. Statics

With relevance to films of four composites of magnetic nanoparticles in dielectric matrices; $(Co)_{0.42}(MgF_2)_{0.58}$, $(Fe_{65}Co_{35})_{0.57}(SiO_2)_{0.43}$, $(Fe_{65}Co_{35})_{0.75}(Al_2O_3)_{0.25}$, $(Fe_{65}Co_{35})_{0.6}(Al_2O_3)_{0.4}$, we have performed numerical investigations of the longitudinal and transverse hysteresis loops, (the hysteresis due to in-the-plane magnetic field longitudinal or transverse with respect to the easy axis). In our simulations, the magnetic-metal inclusions are considered to be identical cubes homogeneously distributed inside a dielectric. The shapes of the inclusions do not play any role since the magnetostatic effects (the shape anisotropies) are completely neglected. Otherwise, the magnetostatics would critically influence the ordering, which is not in line with assumptions of the RMA model, of whom the local-anisotropy and global-anisotropy parameters $k_1 = K_1/\sqrt{N}$, (where $N$ denotes the number of coupled grains), and $K_u$ are the only anisotropy constants including effects of all possible anisotropy origins. From the coercivity measurements, the shape anisotropy of nanoparticles in superferromagnetic composites is known to be inconsistent with that of the isolated nanoparticles, which is due to a smooth change of the magnetic-moment density at the nanoparticle–matrix interfaces (lack of the magnetic surface charges) [19].

Based on literature data (of experiments analyzed within the RMA model), using (2)–(4), we have extracted the sets of material parameters of the films. For $(Co)_{0.42}(MgF_2)_{0.58}$, the constant of randomly oriented uniaxial anisotropy of Co inclusions is $K_1 = 4.5\cdot 10^5$ J/m$^3$, while, the in-the-plane uniform easy-axis anisotropy is reported to take $K_u = 2.0\cdot 10^3$ J/m$^3$. An additional easy-plane anisotropy of the magnetostatic origin is related to the constant $K = -2.0\cdot 10^5$ J/m$^3$. The saturation magnetization and the exchange stiffness for the inclusions and for the matrix are $M_s^{(m)} = 1.4\cdot 10^6$ A/m, $M_s^{(d)} = 2.4\cdot 10^5$ A/m, $A_{ex}^{(m)} = 3.3\cdot 10^{-11}$ J/m, $A_{ex}^{(d)} = 7.3\cdot 10^{-14}$J/m. The average diameter of the magnetic inclusion (the length of edge of the magnetic cube) is $D = 3.3$ nm, which, via a given volume ratio of the metal to dielectric content in the composite, determines the spacing between the surfaces of the closest inclusions $\Lambda = 1.9$ nm, [26,27]. We simulate a square of 166.4nm×166.4 nm of the 15.6 nm-thick film (the thickness of three nanoparticle monolayers), applying the finite-difference method with the grid-discretization size of 0.65nm< $\sqrt{\bar{A}_{ex}/K}$, (we utilize OOMMF package switching the demagnetization field off).

The thickness of the layers is taken to be higher than the effective exchange length of the system $\sqrt{\bar{A}_{ex}}/(K_u^2 + k_1^2)^{1/4} \approx \sqrt{\bar{A}_{ex}/K_u}$. With relevance to the simulations of the dynamical response (next section), for all the studied metal–dielectric films, we have taken quite high value of the Gilbert damping constant $\alpha = 0.1$, which is supported by measurements of composites of FeCo nanoparticles [28–30].

For $(Fe_{65}Co_{35})_{0.6}(Al_2O_3)_{0.4}$, the parameters are following: $K_1 = 1.5\cdot 10^4$ J/m$^3$, $K_u = 5.0\cdot 10^2$ J/m$^3$, $K = -1.4\cdot 10^5$ J/m$^3$, $M_s^{(m)} = 1.9\cdot 10^6$A/m, $M_s^{(d)} = 1.25\cdot 10^5$ A/m, $A_{ex}^{(m)} = 1.7\cdot 10^{-11}$ J/m, $A_{ex}^{(d)} = 3.0\cdot 10^{-14}$ J/m, $D = 2.3$ nm and $\Lambda = 1.2$ nm, [25]. We simulate a square of 182nm×182 nm of the 17.5 nm-thick film (the thickness of five nanoparticle monolayers), with the grid-discretization size of 0.7 nm.

For $(Fe_{65}Co_{35})_{0.75}(Al_2O_3)_{0.25}$, the parameters are following: $K_1 = 1.5\cdot 10^4$ J/m$^3$, $K_u = 2.8\cdot 10^3$ A/m, $K = -1.3\cdot 10^6$J/m$^3$, $M_s^{(m)} = 1.9\cdot 10^6$ A/m, $M_s^{(d)} = 1.0\cdot 10^5$ A/m, $A_{ex}^{(m)} = 1.7\cdot 10^{-11}$ J/m, $A_{ex}^{(d)} = 1.5\cdot 10^{-14}$ J/m, $D = 3.9$ nm and $\Lambda = 1.3$, [25]. We simulate a square of 166.4nm×166.4 nm of the 15.6nm-thick film (the thickness of three nanoparticle monolayers), with the grid-discretization size of 0.65 nm.

For $(Fe_{65}Co_{35})_{0.57}(SiO_2)_{0.43}$, the parameters are following: $K_1 = 1.5\cdot 10^4$ J/m$^3$, $K_u = 2.9\cdot 10^3$ A/m, $K = -5.8\cdot 10^5$ J/m$^3$, $M_s^{(m)} = 1.9\cdot 10^6$ A/m, $M_s^{(d)} = 6.3\cdot 10^5$ A/m, $A_{ex}^{(m)} = 1.7\cdot 10^{-11}$ J/m, $A_{ex}^{(d)} = 1.1\cdot 10^{-13}$J/m, $D = 3.92$ nm and $\Lambda = 2.32$ nm, [31–33]. We simulate a square of 199.68nm×199.68 nm of the 18.72 nm-thick film (the thickness of three nanoparticle monolayers), with the grid-discretization size of 0.78 nm.

The simulations of the hysteresis loops have been performed starting from a zero-field state of the system that is relaxed from the randomly-magnetized state. Domain structures appear despite lack of the magnetostatic interactions as a consequence of the competing complex exchange interactions and RMA. Note that the initial states of our finite systems are not perfectly magnetized in the easy direction. This is because the RMA magnets are "systems with memory", thus, there is a large number of equilibria for any given external field including zero. Properties typical of the reentrant spin glass (overcooled states) have been observed for metal–dielectric nanocomposites [34,35]. The loops of longitudinal and transverse hysteresis, (we mean the hystereses due to the action of in-the-plane field longitudinal or transverse to the easy magnetization direction - $m_x(H_x)$ or $m_y(H_y)$ curves, respectively) are presented in Fig. 1, (we plot halfloops only). For a wide range of the field considered, in majority of the systems, the complete magnetization is not reached, while, the system "remembers" the initial (zero-field) state. Resulting hysteresis curves (except for $(Fe_{65}Co_{35})_{0.75}(Al_2O_3)_{0.25}$) reveal a nonzero slope beyond the loop area (for the field above the coercivity), similar to ones of [36,37].

The coercive fields (of the transverse and longitudinal hysteresis) are found to be relatively low for each of the four materials, however, the strict condition of the soft magnetism, the coercive field of the longitudinal hysteresis lower than 1kA/m is fulfilled by one of the composites only; $(Fe_{65}Co_{35})_{0.6}(Al_2O_3)_{0.4}$. The longitudinal-hysteresis shape for $(Co)_{0.42}(MgF_2)_{0.58}$ is different from those of the $Fe_{65}Co_{35}$-based composites, whereas, the materials of the later group differ significantly from each other in the coercive field.

The transverse hysteresis loops are very narrow (transverse coercivities are low) or even not clearly seen with the field-resolution of Fig. 1. The systems behave similar to the Stoner–Wohlfarth model of the magnetic particle which predicts the absence of the transverse hysteresis and the presence of the rectangular-shaped loop of the longitudinal hysteresis. Some literature on the corresponding nanocomposites reports clearly resolved loops of the transverse hysteresis of the real magnets. They are attributed to large scale of the probed systems, which is related to local deviations of the easy magnetization axis from the average and cannot be reproduced within our simulations. However, the way of the material deposition is crucial in terms of the local distribution of the anisotropy. Specific-angle-oblique sputtering allows for producing

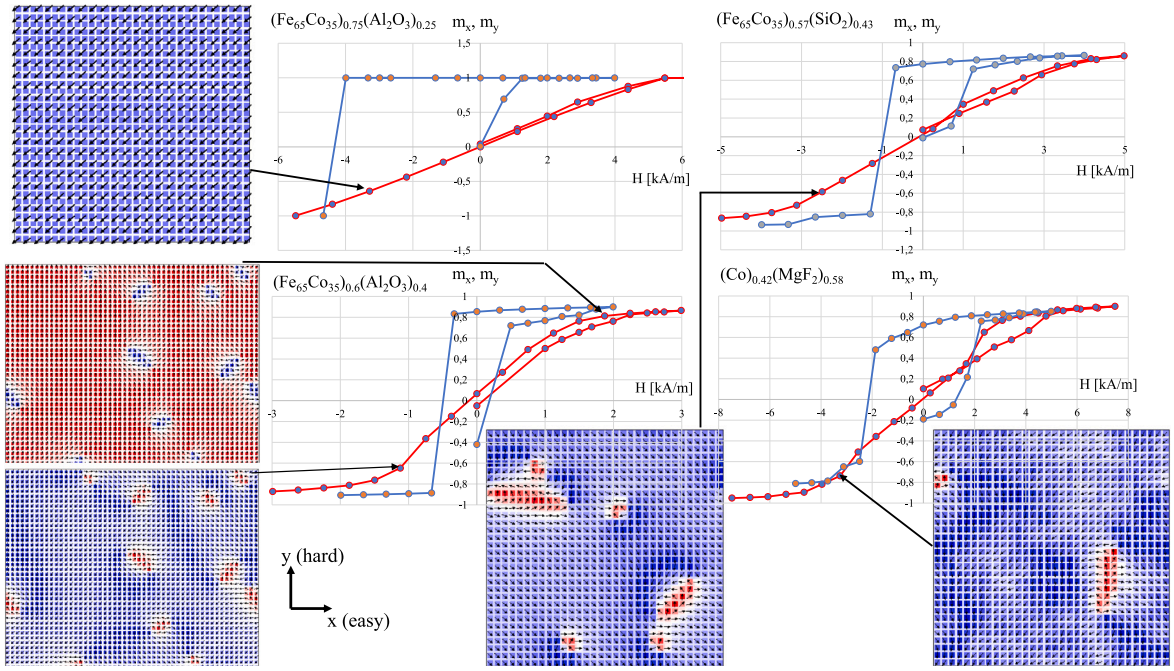


**Fig. 1.** Hysteresis curves $m_x(H_x)$ (blue lines; "longitudinal hysteresis") and $m_y(H_y)$ (red lines; "transverse hysteresis") of the four simulated systems, and snapshots of the magnetization (the colors indicate the direction and intensity of the $m_y$-component) at the indicated points of the "transverse-hysteresis" curve.

nanocomposites of the Stoner–Wohlharth-like hystereses [38]. That hysteresis type is claimed to support the view of dominance of the exchange inter-particle interactions over the dipole–dipole ones [39].

Looking at the snapshots of the transverse component of the magnetization relevant to the transverse reversal modes (Fig. 1), one sees the clearly resolved domains except for $(Co)_{0.42}(MgF_2)_{0.58}$ of whom the random anisotropy is strong enough to prevent uniform demagnetization in the hard plane ($yz$-plane). The strong random anisotropy causes a non-rectangular shape of the longitudinal-hysteresis loop; the remanence magnetization $m_r = M_r/\bar{M}_s$ (called a squareness ratio) of the longitudinal hysteresis loop is visibly-smaller than one. It is not for $Fe_{65}Co_{35}$-based structures, however, there are differences in the remagnetization of particular-composition systems. For the magnetically-hardest of the composites; $(Fe_{65}Co_{35})_{0.75}(Al_2O_3)_{0.25}$, we have found the plot of $m_y(H_y)$ dependence to be a straight line for up to $|m_y| \approx 1$ while the ordering to be uniform (a Stoner–Wohlfarth-like behavior). For magnetically-softer $(Fe_{65}Co_{35})_{0.57}(SiO_2)_{0.43}$ and $(Fe_{65}Co_{35})_{0.6}(Al_2O_3)_{0.4}$, the domain structure is durable against the transverse field and complete magnetization reversal using the transverse field requires the application of a field that exceeds the longitudinal coercivity value, (the corresponding red curves in Fig. 1 differ in shape from the Stoner–Wohlfarth turn). This is related to very narrow minima of the energy of $(Fe_{65}Co_{35})_{0.75}(Al_2O_3)_{0.25}$ compared to the remaining composites. From the comparison of snapshots in Fig. 2(g) and 2 (h), we notice transition between the stripe and maze domains with changing the concentration of the magnetic component, which has been previously observed (using MFM) in superferromagnetic nanocomposites with perpendicular magnetic anisotropy (PMA) [35]. The field-induced shrinking of the stripe domains into the separate bubbles (an incomplete remagnetization in the snapshots of Fig. 1 for the magnetically softer systems) has been observed (with MOKE) for an in-plane-magnetized nanocomposite [37].

## 4. High-frequency dynamics

We have simulated the magnetization dynamics driven with alternating longitudinal, transverse, and in-the-plane rotational field of the microwave frequencies. Correspondingly, the magnetic response can follow from FMR or the oscillatory DW motion or a mixture of both (or a rotational mode of FMR). The driving field is applied to the (zero-field) magnetization states of the beginning points in the hysteresis curves of Fig. 1.

Relatively-strong driving fields are considered, having in mind the composite application to the power conversion. The amplitudes of the flux density in microinductors are typically considered in the range of ~0.01–0.1T [15,40–42], which corresponds, via the permeability of ~100 to the driving field of ~0.1–1.0kA/m.

We neglect the skin effect. Despite a tunneling conductivity is present in real nanocomposites, its value is about four orders of magnitude lower than for bulk metals [26,43–45]. Thus, the potential decrease of the skin depth due to the frequency increase (up to GHz) is compensated by the decrease of the conductivity and the skin depth remains of the μm range [46].

### 4.1. Driving by in-the-plane transverse field

The alternating in-the-plane transverse field drives the oscillations of the magnetization components $m_y$, $m_z$ (perpendicular to the easy axis). For the field amplitude of 0.2 kA/m, we plot the frequency dependence of the response amplitudes of; $(Fe_{65}Co_{35})_{0.75}(Al_2O_3)_{0.25}$ in Fig. 2(a), $(Fe_{65}Co_{35})_{0.6}(Al_2O_3)_{0.4}$ in Fig. 2(d), $(Fe_{65}Co_{35})_{0.57}(SiO_2)_{0.43}$ in Fig. 3(a), and for $(Co)_{0.42}(MgF_2)_{0.58}$ in Fig. 3(d). The square-shaped spatial windows chosen for performing the calculations is pointed out in the snapshots in Figs. 2(g), (h), 3(g). Those single-domain windows are considered in order to simulate conditions of measurement of the dynamical permeability at its maximum (in a single-domain state). In the plots and in the text below, amplitudes of oscillating quantities are denoted as $\mathrm{Amp}(\cdot)$, while, the angular frequency reads $\omega \equiv 2\pi\nu$. For $(Co)_{0.42}(MgF_2)_{0.58}$, the total transverse magnetization of the system is plotted, because of a specific dynamical response of the layer. As seen from the snapshots in Fig. 3j, the out-of-plane component of the magnetization in the layer of $(Co)_{0.42}(MgF_2)_{0.58}$ almost does not oscillate inside the magnetic nanoparticles of the composite except in a small number of them, (unlike in the snapshots of $(Fe_{65}Co_{35})_{0.57}(SiO_2)_{0.43}$ layer for instance, Fig. 3i). Such a behavior does not coincide with the classic description of FMR (by Kittel) and,

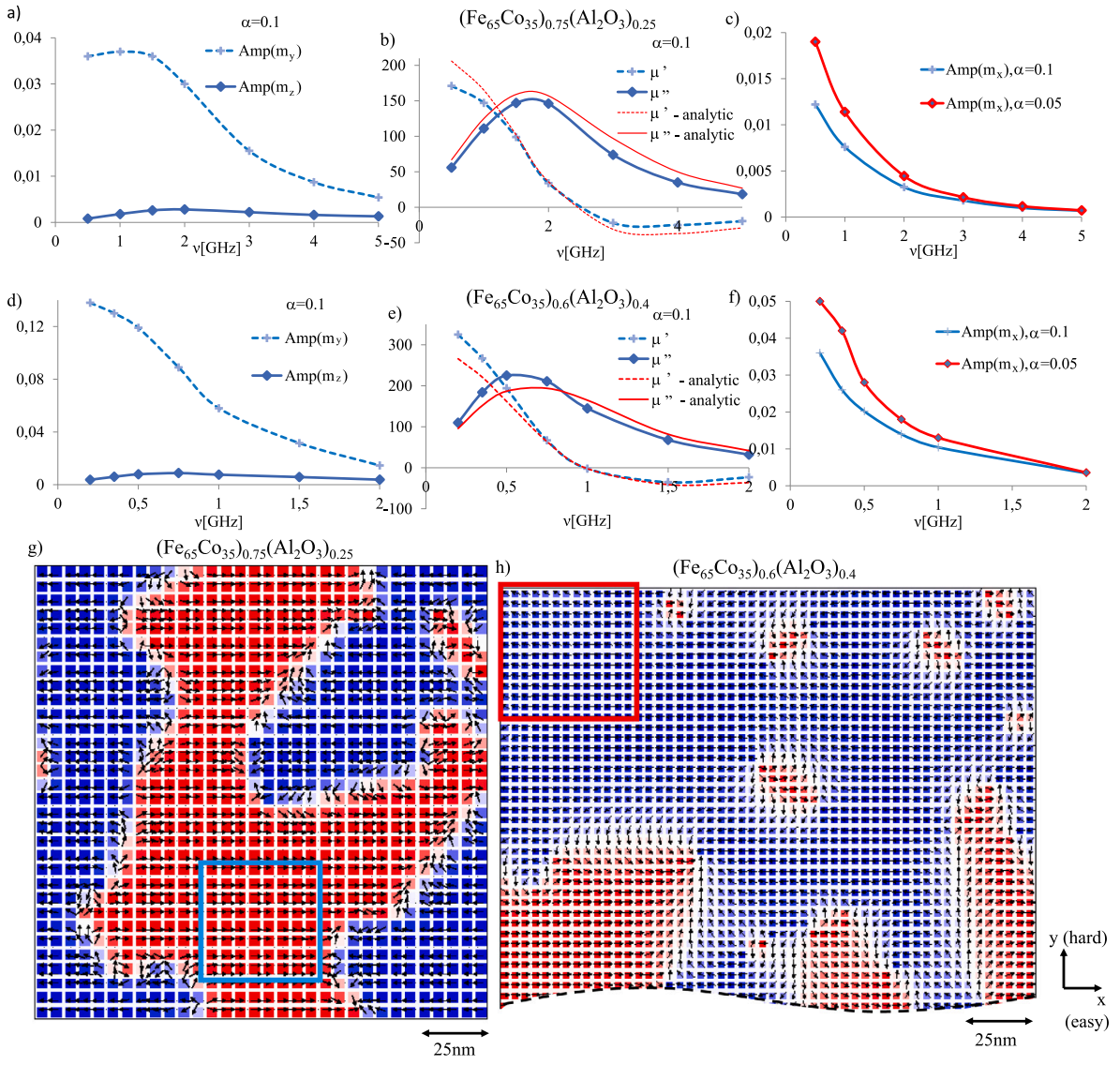


**Fig. 2.** Simulated dynamical response to the alternating transverse field: frequency dependence of the amplitudes of the magnetization components $m_y$, $m_z$ (a), the real and imaginary permeabilities $\mu'$, $\mu''$ (b) for $(Fe_{65}Co_{35})_{0.6}(Al_2O_3)_{0.4}$ layer, and the same for $(Fe_{65}Co_{35})_{0.75}(Al_2O_3)_{0.25}$; (d), (e), respectively. Dynamical response from both the materials to the alternating longitudinal field: frequency dependence of the amplitude of the magnetization component $m_x$; (c), (f). Equilibrium ordering in $(Fe_{65}Co_{35})_{0.75}(Al_2O_3)_{0.25}$; (g), and $(Fe_{65}Co_{35})_{0.6}(Al_2O_3)_{0.4}$; (h). The colors in (g), (h) and their intensity are related to the $m_x$ component of the magnetization. The transverse-field response is established for indicated in (g), (h) spatial windows.

(similar to domain nonuniformity in Section 3), it is due to very strong RMA in $(Co)_{0.42}(MgF_2)_{0.58}$.

Consider FMR due to an alternating field $\mathbf{B}(t)/\mu_0 = [0, H_y(t), 0]$ of an amplitude $\mathrm{Amp}(H_y)$, using the complex dynamical parameter $m_+(t) \equiv m_y(t) + \mathrm{i}m_z(t)$. When considering the single-domain state/area of a ferromagnet, the linearization of (1) around $\mathbf{m} = [1, 0, 0]$ allows one for finding the particular solution in the form $m_+(t) = \left[A_y(\omega) + \mathrm{i}A_z(\omega)\right]\sin(\omega t) + \left[C_y(\omega) + \mathrm{i}C_z(\omega)\right]\cos(\omega t)$ and, via its Fourier transform, the permeability

$$\mu(\omega) \equiv \frac{m_+(\omega)}{H_y(\omega)} = \frac{M_s}{\mathrm{Amp}H_y}\left\{A_y(\omega) + C_z(\omega) + \mathrm{i}\left[A_z(\omega) - C_y(\omega)\right]\right\}. \tag{6}$$

Upon denoting $\omega_1 \equiv \gamma_0\left(\frac{2K_u}{\mu_0 M_s} + M_s\right)$ and $\omega_2 \equiv \gamma_0 \frac{2K_u}{\mu_0 M_s}$, the real and imaginary parts of the permeability read

$$\mu'(\omega) = \gamma_0 M_s \frac{(\omega - \omega_1)\left(\omega^2 - \omega_1\omega_2\right) + \alpha^2\omega^2\left(\omega + \omega_2\right)}{\left(\omega^2 - \omega_1\omega_2\right)^2 + \alpha^2\omega^2\left(\alpha^2\omega^2 + \omega_1^2 + \omega_2^2\right)}$$

$$\mu''(\omega) = \gamma_0 M_s \frac{\alpha\omega\left\{\omega\left[\left(1+\alpha^2\right)\omega - \omega_2\right] - \omega_1\left(\omega - \omega_1\right)\right\}}{\left(\omega^2 - \omega_1\omega_2\right)^2 + \alpha^2\omega^2\left(\alpha^2\omega^2 + \omega_1^2 + \omega_2^2\right)} \tag{7}$$

Zero of $\mu'(\omega)$ and maximum of $\mu''(\omega)$ are close to the FMR frequency $\sqrt{\omega_1\omega_2}$. The angle of the out-of-plane deviation of the magnetization $\delta_\omega$ is directly related to the loss tangent;

$$\tan(\delta_\omega) = \frac{\mathrm{Amp}[m_z](\omega)}{\mathrm{Amp}[m_y](\omega)} = \frac{\mu''(\omega)}{\mu'(\omega)}. \tag{8}$$

Noticing that $\mathrm{Amp}(m_z) \ll \mathrm{Amp}(m_y)$, we verify the application of the FMR description to the nanocomposites via utilizing the relationships $\mu'(\omega) \approx \frac{M_s}{\mathrm{Amp}(H_y)}\mathrm{Amp}[m_y](\omega)\cdot\cos(\delta_\omega)$ and $\mu''(\omega) \approx \frac{M_s}{\mathrm{Amp}(H_y)}\mathrm{Amp}[m_y](\omega)\cdot\sin(\delta_\omega)$. The amplitudes of magnetization components averaged over a spatial window in a single-domain area are determined from the simulations and multiplied by sine or cosine of the calculated with (8) values of $\delta_\omega$. Thus, we evaluate the permeability with dependence on the frequency and compare its plot to the permeability curve calculated with (7), dashed and solid lines in Figs. 2(b), (e), 3(b), respectively. For $(Co)_{0.42}(MgF_2)_{0.58}$, since the dynamics appeared in our simulations to

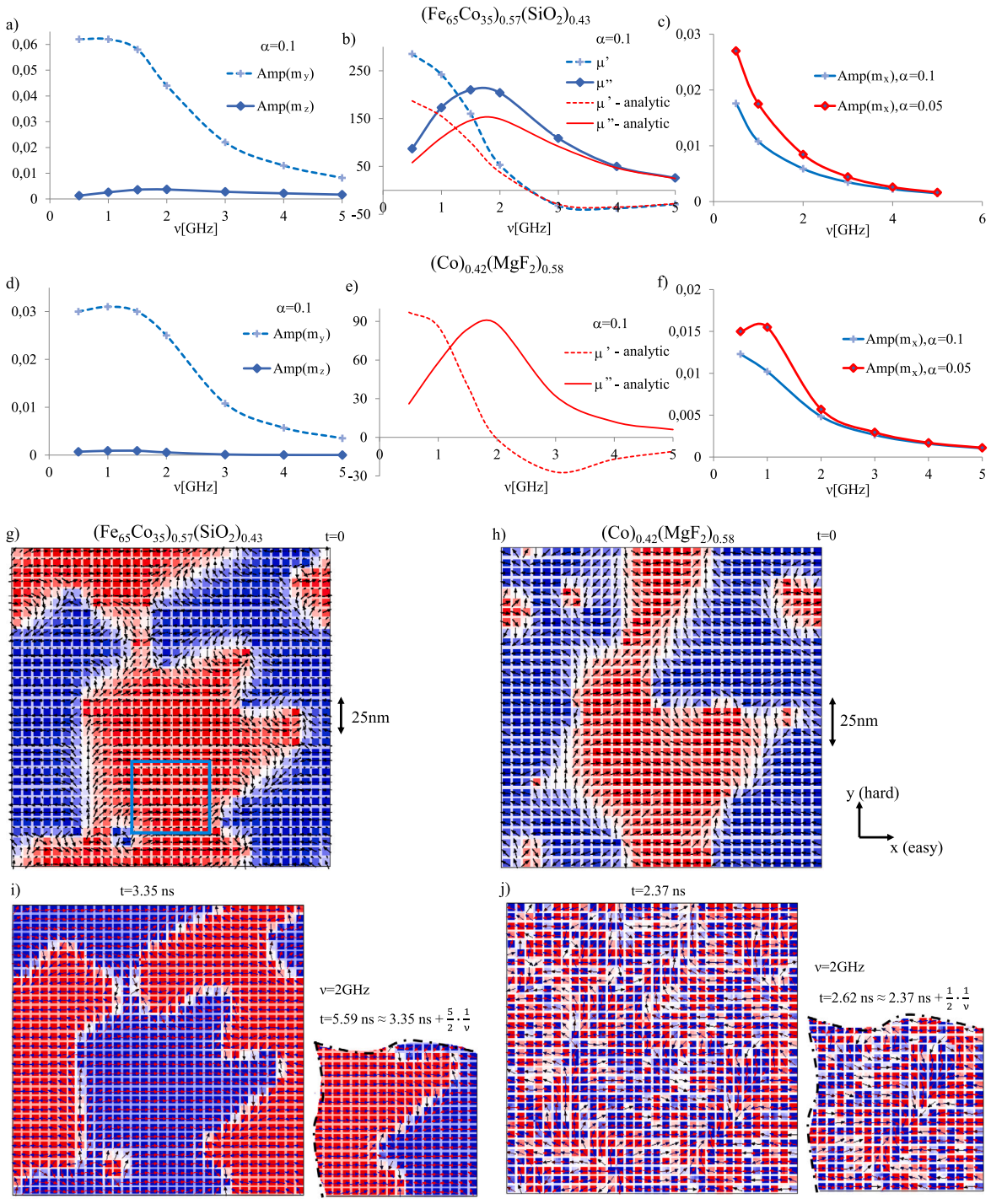


**Fig. 3.** Dynamical response to the alternating transverse field: frequency dependence of the amplitudes of the magnetization components $m_y$, $m_z$ (a), the real and imaginary permeabilities $\mu'$, $\mu''$ (b) for $(Fe_{65}Co_{35})_{0.57}(SiO_2)_{0.43}$ layer, and the same for $(Co)_{0.42}(MgF_2)_{0.58}$; (d), (e), respectively. Dynamical response from both the materials to the alternating longitudinal field: frequency dependence of the amplitude of the magnetization component $m_x$; (c), (f). Equilibrium ordering in $(Fe_{65}Co_{35})_{0.57}(SiO_2)_{0.43}$; (g), and $(Co)_{0.42}(MgF_2)_{0.58}$; (h). The colors in (g), (h) and their intensity are related to the $m_x$ component of the magnetization. The transverse-field response is established for indicated in (g), (h) spatial windows. Bottom line: snapshots of $z$-component of the magnetization during the transverse-field-driven oscillations for $(Fe_{65}Co_{35})_{0.57}(SiO_2)_{0.43}$; (i), (the color intensity is increased via dividing $M_s$ by 1000), and for $(Co)_{0.42}(MgF_2)_{0.58}$; (j), (the color intensity is increased via dividing $M_s$ by 100).

be far from usual FMR as mentioned above, in Fig. 3(e), the analytical permeability curves are plotted only.

While similar, the simulation and analytical curves in Figs. 2(b), (e), 3(b) differ from each other. In Fig. 3(b), (the plot for $(Fe_{65}Co_{35})_{0.57}(SiO_2)_{0.43}$) and in Fig. 2(e), (the plot for $(Fe_{65}Co_{35})_{0.6}(Al_2O_3)_{0.4}$), a relatively large ~ 10% differences in simulation and analytical values of the real part of the low-frequency permeability are found. Such an considerable increase of the real part of the permeability above the analytical value is connected to the breakdown of the Snoek law. Unfortunately, the simulation value of the imaginary part of the permeability is increased compared to the analytical one as well and the loss tangent at sub-GHz frequencies remains large.

Experimental curves of the dynamical permeability for relevant materials are qualitatively similar to ours while, they are better fitted to the analytical curves [28,31]. This is possibly because, the damping

constant is a fitting parameter in the experimental works. The permeability values (so as the damping constant and FMR frequency) can be very strongly influenced by the presence of a substrate and depend on the thickness of the magnet [28]. The most stable in terms of the parameters (and especially similar to our model systems) are multilayered granular films and we have found a good correspondence of the permeability cures for the FeCo-$SiO_2$ composite (Fig. 3(b)) to the experimental data on relevant multilayered system, (up to small differences in the composition and size of the nanoparticles), [47]. Note that low thickness of the interlayer (comparable to the interparticle distances) is crucial for the frequency dependence of the permeability [48].

### 4.2. Driving by longitudinal field and by rotating field

In the system driven with the alternating longitudinal field $\mathbf{B}(t)/\mu_0 = [H_x(t), 0, 0]$, DWs perform the oscillatory motion which leads to the oscillations of the longitudinal magnetization of the system as a whole. For the frequencies close to the resonance point and higher, the driven oscillations of the $m_x$-component of the magnetization are found to be of a very low amplitude. However, according to Figs. 2(c), (f), 3(c), (f), in the sub-GHz range, the oscillations (for $\mathrm{Amp}(H_x) = 0.2$ kA/m) rapidly become significant, of the amplitude comparable to the amplitude of the $m_y$-component when the system is driven with the transverse field of the same amplitude. The increase of the amplitude of the DW oscillations with decreasing the frequency is usual in ferromagnets [49–51]. While frequency of the efficient FMR-based response is limited at the top by the increase of the loss tangent, the frequency of the efficient DW-assisted response is limited at the bottom by the increase of the DW-motion amplitude close to the domain size.

For all the systems, we have found the increase of the longitudinal permeability with decreasing the Gilbert damping constant (Fig. 2(c), (f), 3 (c), (f)). This suggests the related DW motion to be viscous at the certain time scale of the period of oscillations (similar to the constant DW motion below the Walker breakdown). The strongest longitudinal response has been found for $(Fe_{65}Co_{35})_x(Al_2O_3)_{1-x}$ systems. Larger amplitude $\mathrm{Amp}(m_x)$ at the composition factor $x = 0.6$ is compensated be the higher saturation magnetization at $x = 0.75$, hence, the hysteretic losses in both magnets are expected to be similar. Lower amplitude of magnetization oscillations in $(Fe_{65}Co_{35})_{0.75}(Al_2O_3)_{0.25}$ is an advantage with regard to the stability of the domain structure. It allows for the application of stronger driving field than usable for $(Fe_{65}Co_{35})_{0.6}(Al_2O_3)_{0.4}$. However, large volumeric percentage of the metallic phase in the former system is a disadvantage in terms of the requirement of a high resistivity, which is especially important for the case of the DW-assisted response because of the excess losses.

At the microscale, a very strong rotating field can be created with a pair of mutually-perpendicular coils which method is utilized for omnidirectional wireless power transfer [52,53]. Such a field drives the magnetization rotation and possibly causes the overlap of FMR with significant oscillations of the DW positions. For sufficiently-low frequency and high amplitude of the driving field, the response of the layer to (in-the-plane) rotating field becomes nonlinear, which limits the operating ranges of the field frequency and amplitude. We have performed the simulations for the field amplitude of up to 2 kA/m and frequency down to 0.5 GHz for $Fe_{65}Co_{35})_{0.57}(SiO_2)_{0.43}$, $(Co)_{0.42}(MgF_2)_{0.58}$, and for $(Fe_{65}Co_{35})_{0.75}(Al_2O_3)_{0.25}$, roughly establishing that the driven oscillations of in-the-plane components of the magnetization remain sinusoidal in principle, however, for the later system, weakly-visible nonlinear features appear in the plot of $m_x(t)$ in Fig. 4(d) (the blue line).

For the magnetically-softest $(Fe_{65}Co_{35})_{0.6}(Al_2O_3)_{0.4}$, the nonlinear character of the magnetization oscillations in the rotating field of 2kA/m (well above the longitudinal coercive field of Fig. 1 but below the saturating transverse field) is clearly seen in the range of frequencies of our study (see Fig. 4(f), (g)). At 0.2 GHz, instead of the magnetization oscillations, we see in-the-plane rotations of it with some nonlinear features. Notice that in the vicinity of the linear-resonance frequency, at 0.75 GHz, under the strong rotating field of 2kA/m, the magnetization oscillations are chaotic. Thus, there is an upper-limit of the frequency on using the strong rotating field (in the regime of the nonlinear response) to the power conversion. On the other hand, at the relatively-low frequency 0.2 GHz, the amplitudes of the dynamical response have increased from $\mathrm{Amp}(m_y) = 0.14$ at the rotating field 0.2kA/m (or the driving transverse field $\mathrm{Amp}(H_y) = 0.2$kA/m) to $\mathrm{Amp}(m_y) > 0.9$ and $\mathrm{Amp}(m_x) \approx \mathrm{Amp}(m_y)$ at the rotating field of 2kA/m. Such a large oscillation amplitude is related to complete in-the-plane rotations of the magnetization, which we call below a nonlinear rotational mode. The amplitude of the simultaneous out-of-the-plane (nonlinear) oscillations (extracted from Fig. 4(h)) provides an information on the strength of the spin loss (dissipation). The ratio $\eta \equiv \mathrm{Amp}(m_z)/\mathrm{Amp}(m_y) < 0.03$ at the rotating field 2.0kA/m of 0.2 GHz frequency is comparable to one of the linear-response regime, in particular, to the case of the driving with the transverse-field of the amplitude of 0.2kA/m at the same frequency 0.2 GHz.

In Appendix, we apply van der Pol approach to the ferromagnetic nonlinear resonance at the rotating field. Note that, the geometry of our oscillating ferromagnet is different from a widely studied nonlinear-resonant (PMA) system in a rotating in-the-plane field by the presence of an in-the-plane anisotropy [54,55], (we focus on the high-frequency FMR configuration). Despite, established analytical methods to treat the nonlinear resonance are devoted to weakly-nonlinear oscillations which is not the case of $(Fe_{65}Co_{35})_{0.6}(Al_2O_3)_{0.4}$ at 0.2 GHz and 2.0 kA/m for instance, there is a transition between the weak- and strong-nonlinearity regimes with changing the frequency/amplitude of the driving field. Also, in Appendix, simulations of a simplified uniform system of the effective parameters of $(Fe_{65}Co_{35})_{0.6}(Al_2O_3)_{0.4}$ are sketched. We find the highly-nonlinear oscillations at 0.2 GHz in the nanocomposite (Fig. 4(g)) to be well described with the uniform effective model (Fig. 6(e)). At the resonant frequency of 0.75 GHz and the strong rotating field 2.0 kA/m, the magnetization oscillations in the nanocomposite become chaotic (Fig. 4(f)), whereas, some transient (while not chaotic) behavior at the same frequency is found in the uniform model as well (Fig. 6(d)). It should be noted that the transient behavior of the anisotropic ferromagnets under the rotating field has been studied within the Melnikov method in [56], with especial attention to our case of in-the-plane easy-axis anisotropy. However, numerical evaluations were performed in a different range of parameters ($K/K_u \sim 1$, $\alpha = 0.01$) than ours ($K/K_u \sim 100$, $\alpha = 0.1$), which are crucial for values of the Melnikov function.

Evaluating the hysteretic loss, we plot the Zeeman energy with dependence on time in Fig. 5. The Zeeman energy oscillates with the amplitude that corresponds to the average volumeric power loss $\bar{P}_V \sim \mathrm{Amp}(E_Z)$ via

$$\bar{P}_V = \frac{\nu}{V}\int_0^{1/\nu}\left|\frac{dE_Z}{dt}\right|dt. \tag{9}$$

In Fig. 5(a), (b), the time course of the Zeeman energy is shown for $(Fe_{65}Co_{35})_{0.6}(Al_2O_3)_{0.4}$ layer excited by different-amplitude longitudinal fields. The Zeeman-energy amplitude $\mathrm{Amp}(E_Z)$ significantly increases with the field so as the volumeric power loss (the hysteretic loss), from $\bar{P}_V = 20$ W/s·m$^3$·$\nu$ at $|\mathbf{B}|/\mu_0 = 0.2$ kA/m to $\bar{P}_V = 300$ W/s·m$^3$·$\nu$ at $|\mathbf{B}|/\mu_0 = 2$ kA/m). The time dependence of the Zeeman energy of the transverse-field-excited system is plotted in Fig. 5(c), showing a quite large amplitude of the energy oscillations. According to Fig. 5(d), the amplitude of the Zeeman energy (thus, the hysteretic loss) of the system in the rotating field of 2.0 kA/m; ($\bar{P}_V = 80$ W/s·m$^3$·$\nu$) is reduced compared to those in the longitudinal (or even transverse) fields of the amplitude of 2.0kA/m (Fig. 5(b), (c)).

In the present system, the hysteretic losses are comparable or smaller than ones evaluated from data on nanogranular magnets, albeit, to the best of our knowledge, data are available for at least an order of magnitude smaller frequencies than considered here [57]. More

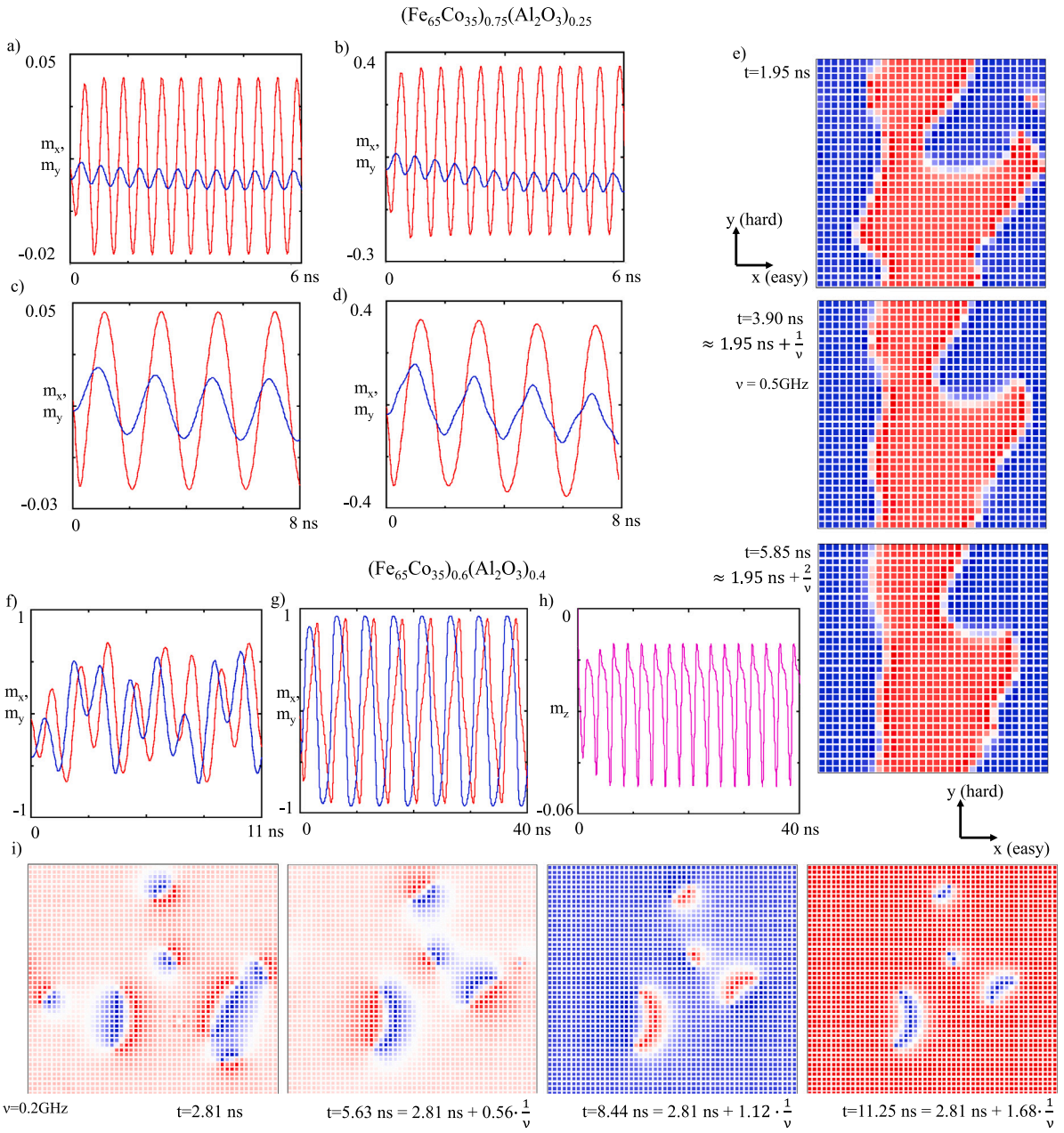


**Fig. 4.** Time dependence of the longitudinal (blue curve) and transverse in-the-plane (red curve) components of the magnetization of $(Fe_{65}Co_{35})_{0.75}(Al_2O_3)_{0.25}$ oscillating in a rotating in-the-plane field of 2 GHz and 0.2kA/m (a), 2 GHz and 2 kA/m (b), 0.5 GHz and 0.2 kA/m (c), 0.5 GHz and 2 kA/m (d) and the snapshots from the later evolution (e). The same for $(Fe_{65}Co_{35})_{0.6}(Al_2O_3)_{0.4}$ at 0.75 GHz and 2 kA/m (f), 0.2 GHz and 2 kA/m (g), with the time dependence of the perpendicular component (h) and the snapshots from the later evolution (i). In the snapshots, the colors indicate the magnetization projection onto the easy axis ($m_x$ component).

importantly, in an alternating (sub-GHz) field of a constant direction, the eddy-current losses are believed to dominate over the hysteretic ones, despite the resistivities of the nanocomposites are large. In the rotating field, our simulations predict the magnetization rotation without or with a minor movement of DWs (see the snapshots in Fig. 5(i)). When, the direction of the domain magnetization is rotating with a constant phase shift with respect to the field and that phase shift is close to $\pi/2$, (the domain magnetization is remaining perpendicular to the field), there is no reason for DWs to move, thus, for inducing the eddy currents. The stability of the domain structure under this high rotating field is confirmed by the time periodicity of the magnetization-component plot in Fig. 4(g). In contrast, the instability of the domain structure in the linearly-polarized (longitudinal or transverse) field of the corresponding amplitude and frequency is seen from the perturbation of the periodicity in the magnetization plots of Fig. 5(b), (c).

## 5. Conclusions

The loss tangent of the transverse-field-driven dynamics has been found to be large for all the $Fe_{65}Co_{35}$-based composites at the GHz and sub-GHz frequencies ($\tan(\delta_\omega) \sim 0.1$ or higher). The transverse-field-driven dynamics of the $(Co)_{0.42}(MgF_2)_{0.58}$ layer does not coincide with the classic description of FMR since, inside magnetic domains, the out-of-plane magnetization component was visibly nonuniform. Therefore, instead the loss tangent, we evaluate the ratio of the amplitudes of the magnetization components $\eta \equiv \mathrm{Amp}(m_z)/\mathrm{Amp}(m_y)$, which is a characteristic of the spin loss as well. At the driving frequency 0.2 GHz

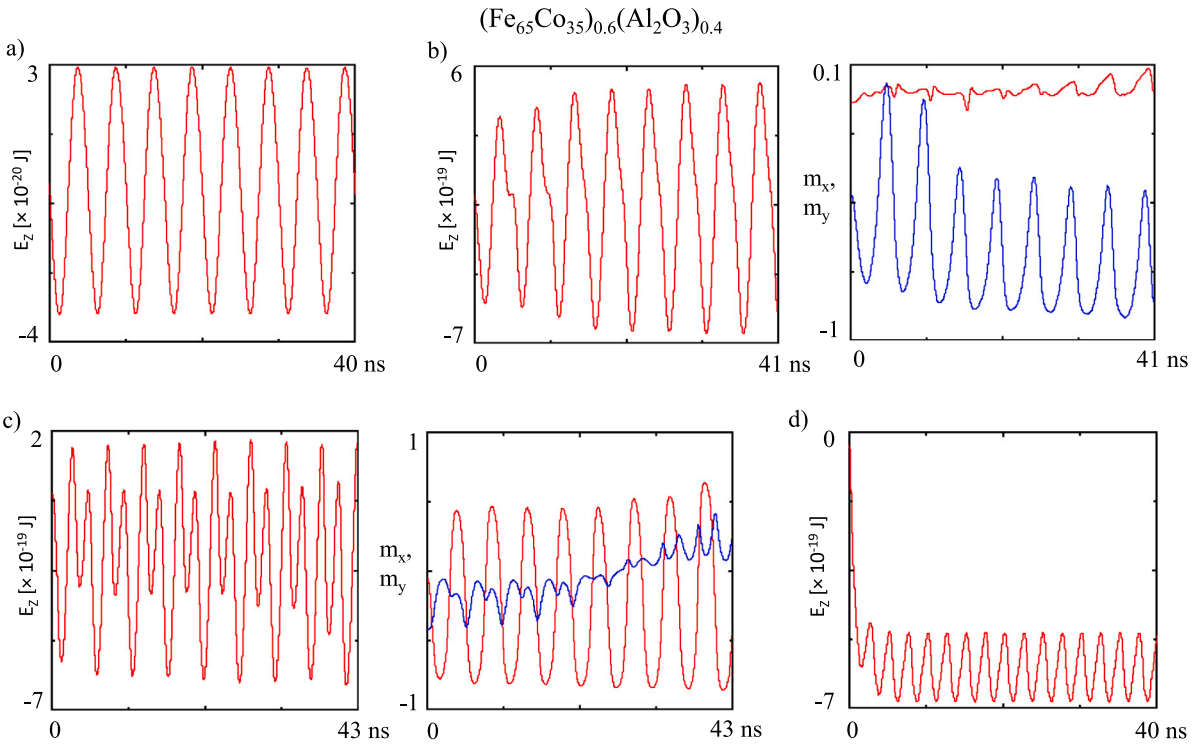


**Fig. 5.** Time dependence of the Zeeman energy of $(Fe_{65}Co_{35})_{0.6}(Al_2O_3)_{0.4}$ under 0.2 GHz alternating field longitudinal to the easy axis of the field amplitude 0.2 kA/m (a), 2.0 kA/m [(b) - left plot], 0.2 GHz alternating field transverse to the easy axis of the field amplitude 2.0 kA/m [(c) - left plot], 0.2 GHz in-the-plane rotating field of 2.0 kA/m (d). Additionally, the time dependence of the magnetization $m_x$ (blue line) and $m_y$ (red line) components of the overall magnetization at the longitudinal [(b) - right plot] and transverse [(c) - right plot] driving field of the amplitude of 2.0 kA/m and frequency 0.2 GHz.

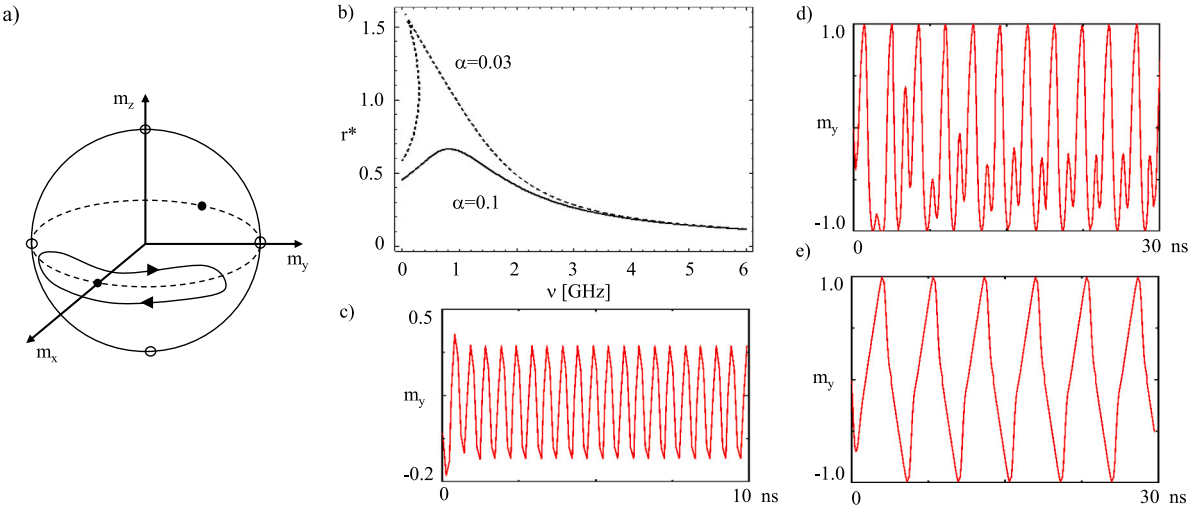


**Fig. 6.** Stable (filled dots) and unstable (open dots) critical points of the LL equation on the unit sphere and a trajectory of the weakly-nonlinear magnetization oscillations (a). Analytically determined equilibrium value of the radius of the phase-space trajectory with dependence on the frequency of the rotating (2 kA/m) field for $(Fe_{65}Co_{35})_{0.6}(Al_2O_3)_{0.4}$, with different Gilbert-damping constants (b), and simulated with a simplified model of $(Fe_{65}Co_{35})_{0.6}(Al_2O_3)_{0.4}$ (a uniform ferromagnet) time dependence of the transverse in-the-plane component ($m_y$) of the magnetization under the 2kA/m rotating field of $\nu = 2$ GHz (c), $\nu = 0.75$ GHz (d), and $\nu = 0.2$ GHz (e).

for $(Fe_{65}Co_{35})_{0.6}(Al_2O_3)_{0.4}$ and at 0.5 GHz for the remaining of the studied systems, $\eta = 0.02 \div 0.05$; (Figs. 2(a), (d), 3(a), (d)). Thus, we have not managed to avoid a relatively high spin loss in the transverse magnetic response at sub-GHz frequencies and the power conversion with the transverse mode of the sub-GHz range is on the limit of efficiency.

Unlike for the cores of large-scale transformers, lowered remanent magnetization $M_r$ (the squareness ratio $m_r \equiv M_r/M_s < 1$, as found for $(Co)_{0.42}(MgF_2)_{0.58}$) is a not an advantage for the microinductors in general. The design of the later includes directing the driving field relative to the axes of the magnetic anisotropy. The requirement of a low anisotropy for the core materials is not applicable to the energy conversion that utilizes FMR. A high (close to one) squareness ratio of the $Fe_{65}Co_{35}$-based composites ensures the DW-assisted dynamical response to the longitudinal field to be the strongest possible, whereas, a close-to-zero surface area of the transverse-hysteresis loops of all the composites studied is related to the largest possible amplitude of the FMR-assisted response to the transverse field.

The longitudinal-field-driven (DW-assisted) response in different composites is found to be significant in the sub-GHz range, while,

rapidly weakening with increase of the frequency. In the field of a given amplitude, the magnetically-softer the system is, (the lower volume of the metallic phase is), the higher amplitude of the DW oscillations is reached. It is due to the increased DW width in the soft magnets, thus, the increased DW mobility, (according to the classic prediction for DW in a constant field by Schryer and Walker [58]). That increase of the DW-oscillation amplitude in $(Fe_{65}Co_{35})_{0.6}(Al_2O_3)_{0.4}$ compensates a decrease of the saturation magnetization relative to $(Fe_{65}Co_{35})_{0.75}(Al_2O_3)_{0.25}$ when evaluating the longitudinal permeability in the regime of the linear response. However maximum of the DW-oscillation amplitude, thus, maximum of the driving field is limited by average size of the domains. Therefore, a lower amplitude of the DW oscillations in the magnetically-hardest $(Fe_{65}Co_{35})_{0.75}(Al_2O_3)_{0.25}$ than in the other layers is noticeable with regard to the stability of the DW structure, whereas, in the magnetically-softest $(Fe_{65}Co_{35})_{0.6}(Al_2O_3)_{0.4}$, the domain-structure instability in a longitudinal field of the amplitude $\mathrm{Amp}(H_x) = 2.0$ kA/m or higher manifests in chaotic oscillations of the magnetization. On the other hand, low volume of the metallic phase in the later system is an advantage in terms of increasing the resistivity, thus, limiting the excess loss of the longitudinal magnetic response.

Periodic rotations of the magnetization in the layer of $(Fe_{65}Co_{35})_{0.6}(Al_2O_3)_{0.4}$ are achievable in a sufficiently-strong rotating field below a frequency of a threshold to the chaotic magnetic response. We have found the amplitude of in-the-plane magnetization oscillations at $|\mathbf{H}| = 2$ kA/m and $\nu = 0.2$ GHz to be higher (the magnetization continuously rotates almost in-the-plane) than the amplitude of $m_y(t)$ at the magnetic response to the transverse field of the corresponding amplitude $\mathrm{Amp}(H_y) = 2$ kA/m. The characteristic of the spin loss of the rotation-excited mode $\eta \approx 0.02$ is comparable to one of the linear (rotational or transverse) excitation modes at the field (or field amplitude) of 0.2 kA/m. Moreover, the nonlinear rotational mode of the magnetization in $(Fe_{65}Co_{35})_{0.6}(Al_2O_3)_{0.4}$ layer is accompanied by a lower hysteretic loss than necessary for exciting the longitudinal mode with the alternating field of equal amplitude. However, the most promising fact about this mode is the dynamical stability of the domain structure in contrast to the case of driving with the strong linearly-polarized (longitudinal or transverse) field. It is related to withholding the excess loss which is the main power loss in the soft magnets at high frequencies. Utilizing the driven rotations of the nanocomposite magnetization seems to be a big chance for increasing the efficiency of the integrated power converters.

## CRediT authorship contribution statement

**Kacper Brzuszek:** Investigation, Validation, Visualization. **Andrzej Janutka:** Conceptualization, Investigation, Supervision, Writing – original draft.

## Declaration of competing interest

The authors declare that they have no known competing financial interests or personal relationships that could have appeared to influence the work reported in this paper.

## Acknowledgment

Calculations have been carried out using resources provided by Wroclaw Centre for Networking and Supercomputing (http://wcss.pl), grant No. 450.

## Appendix. Nonlinear ferromagnetic resonance in a rotating field

Reduce (1) for the case of a homogeneous magnetization into

$$-\frac{\partial \mathbf{m}}{\partial t} = \gamma \mathbf{m} \times (\mathbf{B}_{an} + \mathbf{B}) - \alpha \mathbf{m} \times \frac{\partial \mathbf{m}}{\partial t}, \tag{10}$$

where $\mathbf{B}_{an} = \frac{2K_u}{\bar{M}_s}(\mathbf{m}\cdot\hat{i})\hat{i} - \mu_0 \bar{M}_s(\mathbf{m}\cdot\hat{k})\hat{k}$. At zero external field ($\mathbf{B} = 0$), the critical points of (10) are $\mathbf{m} = [\pm 1, 0, 0]$ or $\mathbf{m} = [0, \pm 1, 0]$ or $\mathbf{m} = [0, 0, \pm 1]$ of whom only those of the first pair (dark dots on the unit sphere in Fig. 6(a)) are stable equilibria. These stability points are of the center type in the case of the absence of the spin dissipation, hence, the surrounding magnetization trajectories should form closed loops (orbits) on the sphere, (Fig. 6(a)).

In order to determine amplitudes of the driven oscillations of the magnetization components in a rotating field, we expand $y$- and $z$-components of Eq. (10) around $\mathbf{m} = [1, 0, 0]$ in $m_y$, $m_z$, up to the third order. We apply the van der Pol transform

$$\begin{aligned} u(t) &= m_y(t)\cos(\omega t) - \sqrt{\frac{\omega_1}{\omega_2}} m_z(t)\sin(\omega t), \\ v(t) &= m_y(t)\sin(\omega t) + \sqrt{\frac{\omega_1}{\omega_2}} m_z(t)\cos(\omega t). \end{aligned} \tag{11}$$

and write down the dynamical equations of u and v. Averaging them over the period of the driving field, thus, exchanging $u \to \tilde{u} \equiv \frac{1}{T}\int_0^T u(t)dt$, $v \to \tilde{v} \equiv \frac{1}{T}\int_0^T v(t)dt$, and transforming the averages into $r \equiv \sqrt{\tilde{u}^2 + \tilde{v}^2}$, $\phi \equiv \arctan(\tilde{v}/\tilde{u})$, one arrives at the autonomous equations

$$\begin{aligned} r\dot{r} &= -\frac{\alpha(\omega_1+\omega_2)}{2(1+\alpha^2)} r^2 - \frac{\sqrt{\omega_1\omega_2}}{8(1+\alpha^2)} \sin(2\phi)\cos(2\phi) r^4 \\ &\quad - \frac{\gamma_0 \mathrm{Amp}(H)}{2(1+\alpha^2)} \sqrt{\frac{\omega_1}{\omega_2}} \frac{\cos(\phi) r}{1 - \frac{1}{8}r^2}, \\ [\tan(\phi)]^{\cdot} &= \omega r^2 + \frac{\sqrt{\omega_1\omega_2}}{1+\alpha^2} r^2 - \frac{3\sqrt{\omega_1\omega_2}}{8(1+\alpha^2)} \cos(2\phi) r^4 \\ &\quad - \frac{\gamma_0 \mathrm{Amp}(H)}{2(1+\alpha^2)} \sqrt{\frac{\omega_1}{\omega_2}} \frac{\sin(\phi) r}{1 - \frac{3}{8}r^2}. \end{aligned} \tag{12}$$

Since $r = \sqrt{m_y^2 + \frac{\omega_1}{\omega_2} m_z^2}$, the critical points $[r^*(\omega), \phi^*(\omega)]$ (the solutions for $\dot{r} = 0$, $\dot{\phi} = 0$) determine the amplitude of the oscillations of the $m_y$-component of the magnetization; $r^*(\omega) = \mathrm{Amp}(m_y)$. In Fig. 6(b), $r^*(\omega)$ is plotted for the parameters $\{\bar{M}_s, K_u\}$ of the $(Fe_{65}Co_{35})_{0.6}(Al_2O_3)_{0.4}$ composite. The plot shows the dependence of $r^*$ on $\omega$ to be unique for the damping constant $\alpha = 0.1$, whereas, a non-uniqueness typical of nonlinear resonance (the transition to chaos) is present for $\alpha \lesssim 0.03$.

We have verified the above analytical predictions on nonlinear FMR simulating the uniform ferromagnetic layer of the parameters $\{\bar{M}_s, K_u, \bar{A}_{ex}\}$ of $(Fe_{65}Co_{35})_{0.6}(Al_2O_3)_{0.4}$ and of $\alpha = 0.1$ in a rotating in-the-plane field, ($\bar{M}_s = 4.8 \cdot 10^5$A/m, $K_u = 5.0 \cdot 10^2$J/m$^3$, $\bar{A}_{ex} = 1.6 \cdot 10^{-11}$J/m). At $\nu = 2$GHz, we have found weakly-nonlinear oscillations of the magnetization whose amplitude coincides quite well with $r^*(2\pi\nu)$, as seen from the comparison of Fig. 6(b) and 6 (c). However, at low frequencies (close to or lower than resonant frequency), the oscillations are not weakly-nonlinear [the formula for $r^*(\omega)$ does not apply anymore and the magnetization vector performs full rotations in the XY-plane instead, (see Fig. 6(d), (e)).

## References

[1] C.R. Sullivan, D.V. Harburg, J. Qiu, C.G. Levey, D. Yao, Integrating magnetics for on-chip power: a perspective, IEEE Trans. Power Electron. 28 (2013) 4342–4353, http://dx.doi.org/10.1109/TPEL.2013.2240465.

[2] M. Araghchini, et al., A technology overview of the PowerChip development program, IEEE Trans. Power Electron. 28 (2013) 4182–4201, http://dx.doi.org/10.1109/TPEL.2013.2237791.

[3] R.J. Kaplar, J.C. Neely, D.L. Huber, L.J. Rashkin, Generation-After-Next Power Electronics: Ultrawide-bandgap devices, high-temperature packaging, and magnetic nanocomposite materials, IEEE Power Electron. Mag. 4 (2017) 36–42, http://dx.doi.org/10.1109/MPEL.2016.2643098.

[4] V. Korenivski, GHz magnetic film inductors, J. Magn. Magn. Mater. 215–216 (2000) 800–806, http://dx.doi.org/10.1016/S0304-8853(00)00292-4.

[5] C.O. Mathuna, N. Wang, S. Kulkarni, S. Roy, Review of integrated magnetics for power supply on chip (PwrSoC), IEEE Trans. Power Electron. 27 (2012) 4799–4816, http://dx.doi.org/10.1109/TPEL.2012.2198891.

[6] E.A. Perigo, B. Weidenfeller, P. Kollar, J. Fuzer, Past, present, and future of soft magnetic composites, Appl. Phys. Rev. 5 (2018) 031301, http://dx.doi.org/10.1063/1.5027045.

[7] D.-S. Xue, F.-S. Li, X.-L. Fan, X.-S. Wen, Bianisotropy picture of higher permeability at higher frequencies, Chin. Phys. Lett. 25 (2008) 4120–4123, http://dx.doi.org/10.1088/0256-307X/25/11/077.

[8] C.-H. Jiang, X.-L. Fan, D.-S. Xue, High frequency magnetic properties of ferromagnetic thin films and magnetization dynamics of coherent precession, Chin. Phys. B 24 (2015) 057504, http://dx.doi.org/10.1088/1674-1056/24/5/057504.

[9] A.N. Lagarkov, K.N. Rozanov, High-frequency behavior of magnetic composites, J. Magn. Magn. Mater. 321 (2009) 2082–2092, http://dx.doi.org/10.1016/j.jmmm.2008.08.099.

[10] S. Ohnuma, H. Fujimori, S. Mitani, T. Masumoto, High-frequency magnetic properties in metal-nonmetal granular films, J. Appl. Phys. 79 (1996) 5130–5135, http://dx.doi.org/10.1063/1.361531.

[11] J.M. Silveyra, E. Ferrara, D.L. Huber, T.C. Monson, Soft magnetic materials for a sustainable and electrified world, Science 362 (2018) eaao0195, http://dx.doi.org/10.1126/science.aao0195.

[12] R.C. Pullar, Hexagonal ferrites: A review of the synthesis, properties and applications of hexaferrite ceramics, Prog. Mater. Sci. 57 (2012) 1191–1334, http://dx.doi.org/10.1016/j.pmatsci.2012.04.001.

[13] D. Polder, J. Smit, Resonance phenomena in ferrites, Rev. Modern Phys. 25 (1953) 89–90, http://dx.doi.org/10.1103/RevModPhys.25.89.

[14] T.N. Lamichhane, L. Sethuraman, A. Dalagan, H. Wang, J. Keller, M.P. Paranthaman, Additive manufacturing of soft magnets for electrical machines–a review, Mater. Today Phys. 15 (2020) 100255, http://dx.doi.org/10.1016/j.mtphys.2020.100255.

[15] D.S. Gardner, G. Schrom, F. Paillet, B. Jamieson, T. Karnik, S. Borkar, Review of on-chip inductor structures with magnetic films, IEEE Trans. Magn. 45 (2009) 4760–4766, http://dx.doi.org/10.1109/TMAG.2009.2030590.

[16] D. Yao, C.G. Levey, R. Tian, C.R. Sullivan, Microfabricated V-groove power inductors using multilayer Co–Zr–O thin films for very-high-frequency DC–DC converters, IEEE Trans. Power Electron. 28 (2013) 4384–4394, http://dx.doi.org/10.1109/TPEL.2012.2233760.

[17] L. Wang, Y. Wang, H. Zhang, Z. Zhong, L. Wang, D. Peng, F. Bai, Integrated on-chip solenoid inductors with nanogranular magnetic cores, IEEE Trans. Magn. 52 (2016) 8400604, http://dx.doi.org/10.1109/TMAG.2015.2514095.

[18] V.N. Kondratyev, H.O. Lutz, Shell effect in exchange coupling of transition metal dots and their arrays, Phys. Rev. Lett. 81 (1998) 4508–4511, http://dx.doi.org/10.1103/PhysRevLett.81.4508.

[19] X. Bao, et al., Excellent microwave absorption of FeCo/ZnO composites with defects in ZnO for regulating the impedance matching, J. Alloys Compd. 769 (2018) 512–520, http://dx.doi.org/10.1016/j.jallcom.2018.08.036.

[20] S.A. Makhlouf, F.T. Parker, F.E. Spada, A.E. Berkowitz, Magnetic anomalies in NiO nanoparticles, J. Appl. Phys. 81 (1997) 5561–5563, http://dx.doi.org/10.1063/1.364661.

[21] R. Alben, J.J. Becker, M.C. Chi, Random anisotropy in amorphous ferromagnets, J. Appl. Phys. 49 (1978) 1653–1658, http://dx.doi.org/10.1063/1.324881.

[22] G. Herzer, Grain size dependence of coercivity and permeability in nanocrystalline ferromagnets, IEEE Trans. Magn. 26 (1990) 1397–1402, http://dx.doi.org/10.1109/20.104389.

[23] K. Suzuki, G. Herzer, J.M. Cadogan, The effect of coherent uniaxial anisotropies on the grain-size dependence of coercivity in nanocrystalline soft magnetic alloys, J. Magn. Magn. Mater. 177 (1998) 949–950, http://dx.doi.org/10.1016/S0304-8853(97)00987-6.

[24] G. Herzer, Modern soft magnets: Amorphous and nanocrystalline materials, Acta Mater. 61 (2013) 718–734, http://dx.doi.org/10.1016/j.actamat.2012.10.040.

[25] S. Wang, J. Ma, X. Zhang, J. Li, Magnetic softness and interparticle exchange interactions of $(Fe_{65}Co_{35})_{1x}(Al_2O_3)_x$ (x = 0 – 0.50) nanogranular films, Thin Sol. Films 520 (2012) 5046–5052, http://dx.doi.org/10.1016/j.tsf.2012.03.025.

[26] K.D. Coonley, G.J. Mehan, C.R. Sullivan, U.J. Gibson, Evaporatively deposited Co-$MgF_2$ granular materials for thin-film inductors, IEEE Trans. Magn. 36 (2000) 3463–3465, http://dx.doi.org/10.1109/20.908861, http://dx.doi.org/10.1063/1.2190719.

[27] V. Ionescu, M. Osiac, C.P. Lungu, O.G. Pompilian, I. Jepu, I. Mustata, G.E. Iacobescu, Morphological and structural investigations of Co-$MgF_2$ granular thin films grown by thermionic vacuum arc, Thin Sol. Films 518 (2010) 3945–3948, http://dx.doi.org/10.1016/j.tsf.2010.02.035.

[28] G. Lu, H. Zhang, J.Q. Xiao, X. Tang, Z. Zhong, F. Bai, High-frequency properties and thickness-dependent damping factor of – thin films, IEEE Trans. Magn. 48 (2012) 3654–3657, http://dx.doi.org/10.1109/TMAG.2012.2200096.

[29] S. Wang, X. Zhang, J. Li, J. Ma, J. Huang, Enhanced magnetic softness and high-frequency characteristics of $Fe_{51.1}Co_{48.9}B$-$Al_2O_3$ nanogranular films, Scr. Mater. 65 (2011) 45–48, http://dx.doi.org/10.1016/j.scriptamat.2011.03.010.

[30] Y. Wang, H. Zhang, D. Wen, Z. Zhong, F. Bai, Magnetic and high frequency properties of nanogranular CoFe-$TiO_2$ films, J. Appl. Phys. 113 (2013) 17A316, http://dx.doi.org/10.1063/1.4795325.

[31] S. Ge, D. Yao, M. Yamaguchi, X. Yang, H. Zuo, T. Ishii, D. Zhou, F. Li, Microstructure and magnetism of FeCo-$SiO_2$ nano-granular films for high frequency application, J. Phys. D: Appl. Phys. 40 (2007) 3660–3664, http://dx.doi.org/10.1088/0022-3727/40/12/016.

[32] D. Yao, S. Ge, X. Zhou, H. Zuo, Grain size dependence of coercivity in magnetic metal–insulator nanogranular films with uniaxial magnetic anisotropy, J. Appl. Phys. 107 (2010) 073902, http://dx.doi.org/10.1063/1.3357399.

[33] X. Ou, J. He, Z. Xia, J. An, J. Hao, S. He, D. Zhao, Fabrication and magnetic properties of strip-patterned FeCoB-$SiO_2$ nanoparticle films for GHz application, Mater. Sci. Eng. B 242 (2019) 69–74, http://dx.doi.org/10.1016/j.mseb.2019.03.009.

[34] W. Kleemann, O. Petracic, Ch. Binek, G.N. Kakazei, Yu.G. Pogorelov, J.B. Sousa, S. Cardoso, P.P. Freitas, Interacting ferromagnetic nanoparticles in discontinuous $Co_{80}Fe_{20}$-$Al_2O_3$ multilayers: From superspin glass to reentrant superferromagnetism, Phys. Rev. B 63 (2001) 134423, http://dx.doi.org/10.1103/PhysRevB.63.134423.

[35] A.A. Stashkevich, et al., Brillouin light scattering observation of the transition from thesuperparamagnetic to the superferromagnetic state in nanogranular ($SiO_2$)Co films, J. Appl. Phys. 104 (2008) 093912, http://dx.doi.org/10.1063/1.3009339.

[36] S. Bedanta, et al., Superferromagnetic domain state of a discontinuous metal insulator multilayer, Phys. Rev. B 72 (2005) 024419, http://dx.doi.org/10.1103/PhysRevB.72.024419.

[37] N. Chowdhury, S. Bedanta, S. Sing, W. Kleemann, Controlling the size and relaxation dynamics of superferromagnetic domains, J. Appl. Phys. 117 (2015) 153907, http://dx.doi.org/10.1063/1.4918670.

[38] Y. He, Y. Wang, Z. Zhong, H. Zhang, F. Bai, High-frequency magnetic loss in nanogranular FeCoTiO films with different histories of induced uniaxial anisotropy, IEEE Trans. Magn. 54 (2018) 2800905, http://dx.doi.org/10.1109/TMAG.2018.2842430.

[39] S.M. Ryabchenko, A.A. Timopheev, V.M. Kalita, A.F. Lozenko, P.A. Trotsenko, V.A. Stephanovich, M. Munakata, Intergranular interactions in nanogranular $(CoFeB)_x$-$(SiO_2)_{1x}$ films with temperature and angular variations in coercivity, Low Temp. Phys. 36 (2010) 682–692, http://dx.doi.org/10.1063/1.3490833.

[40] G.R. Khan, C.R. Sullivan, Nanogranular nickel iron thin films for high frequency power applications, in: Proc. of 2013 Twenty-Eighth Annual IEEE Appl. Power Electronics Conf. and Expo, APEC, 2013, pp. 1638–1643, http://dx.doi.org/10.1109/APEC.2013.6520516.

[41] A.J. Hanson, J.A. Belk, S. Lim, C.R. Sullivan, D.J. Perreault, Measurements and performance factor comparisons of magnetic materials at high frequency, IEEE Trans. Power Electron. 31 (2016) 7909–7925, http://dx.doi.org/10.1109/TPEL.2015.2514084.

[42] Y. He, Z. Zhang, R. Wu, W. Guo, H. Zhang, F. Bai, On-chip coupled inductors with a novel spliced anisotropic and isotropicmagnetic core for inductance and coupling enhancement, Sol. State. Electron. 164 (2020) 107699, http://dx.doi.org/10.1016/j.sse.2019.107699.

[43] P. Zukowski, T. Koltunowicz, J. Partyka, Yu.A. Fedotova, A.V. Larkin, Electrical properties of nanostructures $(CoFeZr)_x$+$(Al_2O_3)_{1-x}$ with use of alternating current, Vacuum 83 (2009) S275–S279, http://dx.doi.org/10.1016/j.vacuum.2009.01.081.

[44] W. Li, Y. Sun, C.R. Sullivan, High-frequency resistivity of soft magnetic granular films, IEEE Trans. Magn. 41 (2005) 3283–3285, http://dx.doi.org/10.1109/TMAG.2005.854720.

[45] K. Ikeda, T. Suzuki, T. Sato, FeNiSiO/$SiO_2$ multi-layer granular magnetic films with high-resistivity, Trans. Mater. Res. Soc. Jpn. 934 (2009) 9–13, http://dx.doi.org/10.14723/tmrsj.34.9.

[46] L.Z. Wu, J. Ding, H.B. Jiang, C.P. Neo, L.F. Chen, C.K. Ong, High frequency complex permeability of iron particles in a nonmagnetic matrix, J. Appl. Phys. 99 (2006) 083905.

[47] K. Ikeda, T. Suzuki, T. Sato, CoFeSiO/$SiO_2$ multilayer granular films with very narrow ferromagnetic resonant linewidth, IEEE Trans. Magn. 45 (2009) 4290–4293, http://dx.doi.org/10.1109/TMAG.2009.2023616.

[48] H. Geng, et al., Soft magnetic property and high-frequency permeability of $[Fe_{80}Ni_{20}$–O/$TiO_2]_n$ multilayer thin films, J. Alloys Compd. 576 (2013) 13–17, http://dx.doi.org/10.1016/j.jallcom.2013.04.128.

[49] A. Janutka, K. Brzuszek, Domain-wall-assisted giant magnetoimpedance of thin-wall ferromagnetic nanotubes, J. Magn. Magn. Mater. 465 (2018) 437–449, http://dx.doi.org/10.1016/j.jmmm.2018.06.007.

[50] A. Janutka, K. Brzuszek, Domain-wall-assisted asymmetric magnetoimpedance in ferromagnetic nanostripes, J. Phys. D: Appl. Phys. 52 (2019) 035003, http://dx.doi.org/10.1088/1361-6463/aae6b4.

[51] A. Janutka, K. Brzuszek, Giant magnetoreactance in magnetic nanowires, J. Magn. Magn. Mater. 515 (2020) 167297, http://dx.doi.org/10.1016/j.jmmm.2020.167297.

[52] L. Xie, Y. Shi, Y.T. Hou, W. Lou, Wireless power transfer and applications to sensor networks, IEEE Wirel. Commun. 20 (2013) 140–145, http://dx.doi.org/10.1109/MWC.2013.6590061.

[53] B.-J. Che, G.-H. Yang, F.-Y. Meng, K. Zhang, J.-H. Fu, Q. Wu, L. Sun, Omnidirectional non-radiative wireless power transfer with rotating magnetic field and efficiency improvement by metamaterial, Appl. Phys. A 116 (2014) 1579–1586, http://dx.doi.org/10.1007/s00339-014-8409-0.

[54] H. Suhl, The nonlinear behavior of ferrites at high microwave signal levels, Proc. IRE 44 (1956) 1270–1284, http://dx.doi.org/10.1109/JRPROC.1956.274950.

[55] G. Bertotti, C. Serpico, I.D. Mayergoyz, Nonlinear magnetization dynamics under circularly polarized field, Phys. Rev. Lett. 86 (2001) 724–727, http://dx.doi.org/10.1103/PhysRevLett.86.724.

[56] C. Serpico, M. d'Aquino, A. Quercia, S. Perna, I.D. Mayergoyz, Transient chaos in nanomagnets subject to elliptically polarized AC applied fields, IEEE Trans. Magn. 55 (2019) 4300305, http://dx.doi.org/10.1109/TMAG.2018.2865574.

[57] G. Khan, Design and Synthesis of Soft Magnetic Materials for High Frequency Power Applications, ProQuest Dissertations Publishing, 2013, 1553172.

[58] N.L. Schryer, L.R. Walker, The motion of 180° domain walls in uniform dc magnetic fields, J. Appl. Phys. 45 (1974) 5406–5421, http://dx.doi.org/10.1063/1.1663252.